Journal of Materials Chemistry C

Accepted Manuscript

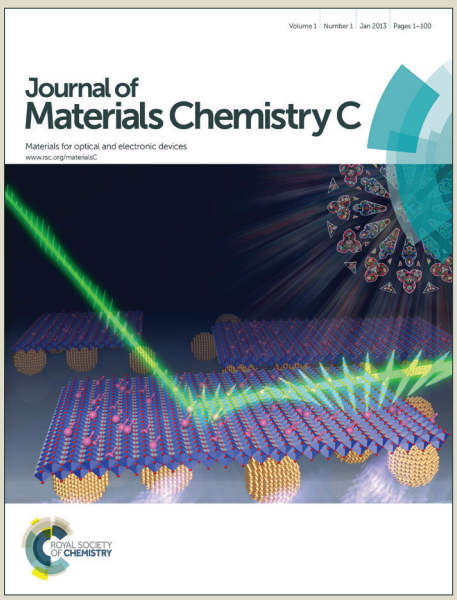

ROYAL SOCIETY OF CHEMISTRY

www.rsc.org/materialsC

Self-assembled Buffer Layer from Conjugated Diblock Copolymers with Ethyleneoxide Side Chains for High Efficiency Polymer Solar Cells

Yueqin Shi[1], Licheng Tan[1], Lie Chen[1], Yiwang Chen[*1,2]

[1]Institute of Polymers/Department of Chemistry, Nanchang University, 999 Xuefu Avenue, Nanchang 330031, China; [2]Jiangxi Provincial Key Laboratory of New Energy Chemistry, Nanchang University, 999 Xuefu Avenue, Nanchang 330031, China

Abstract

In this article, we present a novel and promising approach to promote the device performance and stability by the simple incorporation of all conjugated polythiophene diblock copolymer, poly(3-hexylthiophene)-b-poly(3-triethylene glycol thiophene) (P3HT-b-P3TEGT), into the active layer based on inverted device structures. During spin-coating process, the triethylene glycol side chains of P3HT-b-P3TEGT would spontaneously vertically migrate to the active layer surface and form nanoscale self-assembled anode buffer layer, which simultaneously drive the orderly packing of donor polymer chains and vertical phase separation morphology, allowing electrons and holes to move more efficiently to respective electrode. Meanwhile, the nanoscale self-assembled buffer layer can form interfacial modification and ohmic contact between the active layer and Ag (or MoO_3/Ag) electrode, reduce the contact resistance of the device, and increase the electrical conduction of the device, especially upon chelating lithium ions (Li^+) to the triethylene glycol side chains of P3HT-b-P3TEGT. Combining the above advantages, the efficiency and stability of polymer solar cells are enhanced. A remarkable improvement in the PCE with 7.3 % (measured in air) is obtained for PBDTTT-C-T:PC_{71}BM devices.

Keywords: diblock copolymer; self-assembly; anode buffer layer; lithium ions; polymer solar cells

Introduction

* Corresponding author. Tel.: +86 791 83969562; fax: +86 791 83969561. *E-mail address*: ywchen@ncu.edu.cn (Y. Chen).

Bulk heterojunction (BHJ) polymer solar cells (PSCs) based on an active layer composed of a conjugated polymer as the donor and fullerene derivative as the acceptor have gained increasing attention for their ease of fabrication, mechanical flexibility, light weight, and low-cost fabrication of large-area devices. During the past decades, extensive efforts are focused on the improvement of the power conversion efficiency (PCE) and device stability for economically viable applications by molecular structure engineering[1-2], morphology control[3-5], and device optimization[6-10]. So far, the highest reported PCE of PSCs has approached 10%[11-17]. The most common conjugated polymer for donor and acceptor materials are poly(3-hexylthiophene) (P3HT) and [6,6]-phenyl-C_{61}-butyric acid methyl ester ($PC_{61}BM$). But their performance is limited for the low short circuit current (J_{sc}) and open-circuit voltage (V_{oc}) originating from the relative wide band gap of P3HT donor and low energy of lowest unoccupied molecular orbital (LUMO) of $PC_{61}BM$.

To enhance the PCE, the lower band gap copolymers instead of P3HT and a higher LUMO energy acceptor material were considered. In addition, the morphology control of active layer is also processed to increase the efficiency, such as thermal annealing[22], solvent annealing[23], additives[24-27, 28], and solvent mixture[29-30]. These techniques have been proven to be very effective to obtain lateral nanoscale phase-separated structures (the phase separation size is equal to the exciton diffusion length). Especially, it should be noted that the nanoscale vertical phase segregation morphology of active layer is equally critical for the enhancement of PCE. The vertical components' distribution, i.e. the p-type copolymers donor are rich near the high work function (WF) anode and n-type acceptor materials are rich near the low WF metal cathode, can form an efficient pathway for the carriers transfer and allows electrons and holes moving to the cathode and anode more efficiently, respectively[31, 32].

On the other hand, in order to achieve high-performance BHJ PSCs, interfacial engineering of OPVs is another important approach. In BHJ PSCs, to decrease the energy barriers for electron- and hole-extraction, WF of cathode and anode should match the acceptor's LUMO and donor's highest occupied molecular orbital (HOMO) well, respectively. The energy barriers between electrodes and the active layer could often be reduced effectively by inserting buffer layers at the cathode/anode. Over the past years, much efforts had been spent in exploring a material that could act as an efficient hole extraction layer for BHJ PSCs. The anode buffer layer should form

an ohmic contact at the interface between the active layer and anode electrode, and possess higher WF and higher hole mobility for hole transportation and collection[33]. From these points of view, it is a wise choice for thiophene derivatives as hole transport layer (HTL) to provide an ohmic contact with the donor material[34-35]. Traditionally, the buffer layer is fabricated into the device by an additional step. However, such additional process will complicate the device fabrication processes, consequencely, increase the cost.

To achieve the nanoscale vertical phase segregation morphology of active layer, and meanwhile, to obtain the buffer layer without additional spin-coating process, the self-assembled buffer layer is utilized in the BHJ PSCs. It had been reported that a fullerene derivative (F-PCBM) as buffer layer between cathode and active layer could improve the performance of BHJ PSC resulting from the spontaneous surface segregation of fluorocarbon chains onto the surface of active layer[36]. Besides, the vertical phase separation and self-assembled buffer layer via spontaneously migration of PEG to the top could also be obtained for efficient and air-stable PSCs by blending the poly(ethylene glycol) (PEG) molecules or fullerene-end-capped PEG (PEG-C_{60}) into the photoactive layer[33, 36-39].

In addition, compared with conventional BHJ PSCs, inverted-type devices exhibited better long-term ambient stability by avoiding the need for corrosive and hygroscopic hole-transporting poly(3,4-ethylenedioxylenethiophene):poly(styrenesulphonic acid) (PEDOT:PSS) and low WF metal cathode, both of which were harmful to device lifetime.

Here we demonstrated an interesting and promising way to improve the performance and air stability of PSCs based on inverted device structures ITO/ZnO/active layer/Ag (or MoO_3/Ag) by introducing the poly(3-hexylthiophene)-b-poly(3-triethylene glycol thiophene) (P3HT-b-P3TEGT), an all diblock copolymer containing polythiophene derivative segments whose side chain was triethylene glycol, into the P3HT:PC_{61}BM or PBDTTT-C-T:PC_{71}BM active layers. During the spin-coating and solvent evaporation process, the P3HT-b-P3TEGT would spontaneously self-segregate onto the film and form the nanoscale self-assembled buffer layers due to the vertical migration of triethylene glycol side chains to the active layers' surface. The chain orientation of P3HT-b-P3TEGT at the surface would also force the donor copolymer chains in the active layer to adopt the same orientation due to the high crystallinity of copolymer donors and simultaneously induce the vertical phase segregation morphology of

active layer. Furthermore, the presence of triethylene glycol side chains between the active layer and anode electrode (Ag or MoO_3/Ag) would form an amphiphilic interface, decreasing the energy barriers for hole collection and forming an ohmic contact, especially upon chelating lithium ion (Li^+) to the triethylene glycol side chains of P3HT-b-P3TEGT (P3HT-b-P3TEGT:Li^+), leading to the further enhancement of device performance and stability.

Results and Discussion

The P3HT-b-P3TEGT diblock copolymers were synthesized following the procedure of McCullough and co-workers[40] successfully (**Supporting Information**). And the resulting copolymers were purified by sequential soxhlet extraction using methanol, acetone, hexane and chloroform solvents. The weight ratios of two blocks were determined to be 8:1, 4:1 and 2:1 (P3HT:P3TEGT) using ^{1}H NMR spectroscopy, so we also abbreviated these diblock copolymers (P3HT-b-P3TEGT) as H8T1, H4T1 and H2T1 in data, which were reported in our previous work [41]. The gel permeation chromatography (GPC) using tetrahydrofuran (THF) as the eluent were processed to estimate number-average molecular weight (M_n) of the diblock copolymers. When the P3HT-b-P3TEGT or P3HT-b-P3TEGT:Li^+ diblock copolymer was added to the P3HT:PC_{61}BM or PBDTTT-C-T:PC_{71}BM active layers, it would spontaneously migrate to the surface and form the nanoscale self-assembled buffer layer between active layer and Ag or MoO_3/Ag anode electrode, simultaneously inducing the orientation of donor copolymer chains and vertical distribution of active layer components (**Scheme 1**).

To investigate the vertical surface segregation of P3HT-b-P3TEGT during spin coating process, X-ray photoelectron spectroscopy profiles (XPS) was conducted in **Figure 1**. The films were all prepared on ZnO coated-ITO glass substrates by spin-coating the P3HT:PC_{61}BM solutions blended with various concentration of H4T1, pure Li^+ and 0.6 mg/mL H4T1 chelated with Li^+ ion (H4T1:Li^+) with a fixed concentration of P3HT at 20 mg/mL. It was observed that the peak of O 1s at 531.8 eV became stronger with the gradually increasing of H4T1 amount and even showed a slight red-shift of the H4T1:Li^+, which could be belonged to the chelation of the triethylene glycol side chains with Li^+[42-45]. Besides, the Li 1s spectra showed that the intensity of the peaks at 49.3 eV and 63.3 eV, resulting from the Li^+ salt, became stronger with the addition of Li^+ salt into the P3HT:PC_{61}BM solution, especially for the P3HT:PC_{61}BM:H4T1:Li^+

film. The O/C atomic ratios calculated from the copolymer blend compositions in solution and measured from the XPS results of films surface were plotted as a function of the H4T1 concentration. From the results, the O/C ratios of the films' surface measured from the XPS results displayed much higher than the calculated ratio from the copolymer blend compositions for all the concentrations, revealing the vertical migration of H4T1 or H4T1:Li^+ to the film surface during the spin-coating process. When the concentration of H4T1 increased to ~ 0.6 mg/mL, the O/C atomic ratio (measured by the XPS) attained the saturated point, which was consistent with the results of water contact angles in **Figure S1** (**Supporting Information**)[46]. On the other hand, the H8T1 and H2T1 diblock copolymers also demonstrated the saturated point at the concentration of ~ 1.2 mg/mL and ~ 0.3 mg/mL, respectively. The saturation behavior was also observed in our previous work on self-organized HTLs based on a fluorinated side chains diblock copolymers[10]. The active layer surface was almost covered by triethylene glycol side chains of P3HT-b-P3TEGT diblock copolymers completely above the saturated point. In addition, the thickness of P3HT:PC_{61}BM, P3HT:PC_{61}BM:P3HT-b-P3TEGT and P3HT:PC_{61}BM:P3HT-b-P3TEGT:Li^+ films calculated from AFM analysis were all 100 nm approximately in **Figure S2**, revealing that the buffer layer segregated on the surface of active layer was a very thin layer, which might be even monolayer or several layers thickness.

---------- Figure 1 ---------

We optimized the electrical and optical characterizations of P3HT:PC_{61}BM:H4T1 active layer by changing the concentration of H4T1 in 1,2-dichlorobenzene (DCB) solution using the UV-vis absorption and X-ray diffraction (XRD) measurements. The normalized absorption spectra of the polymer films spin-coated from DCB solution (**Figure S3**) were similar and showed the absorption band of thiophene chains was appeared at about 510, 560 and 610 nm, and PC_{61}BM at 330 nm, respectively. Compared with the pristine P3HT:PC_{61}BM film, the absorption peaks of thiophene chains in P3HT:PC_{61}BM:H4T1 films was somewhat red-shifted with 6 nm approximately and simultaneously a stronger absorption at 610 nm, while the absorption peak of PC_{61}BM displayed no shift, demonstrating the active layer had organized into supermolecular assemblies and formed an increasing planarity, even more ordering and higher crystalline of the packed P3HT chains induced by the orientation of surface segregation of H4T1. To further testify the ordering and crystalline of thiophene chains, the X-ray

diffraction (XRD) was monitored (**Figure 2**). The XRD results revealed that the introduction of H4T1 or H4T1:Li^+ into P3HT:$PC_{61}BM$ system could improve the crystalline and ordered structures of P3HT in the active layer. The pristine P3HT:$PC_{61}BM$ film showed a diffraction peak at $2\theta \approx 5.4^o$, corresponding to *d*-spacing of 16.3 Å of P3HT. After the introduction of H4T1 or H4T1:Li^+ into P3HT:$PC_{61}BM$ solution, the *d*-spacing peaks were all shifted slightly, which was expanded by ~1.0 Å. It was more interesting that a new diffraction peak appeared at $2\theta \approx 6.5^o$ (*d*-spacing of ~13.58 Å) in the ternary blends, which probably derived from self-assembly of thiophene chains of copolymers in the active layer. Besides, the results also indicated the P3HT polymer chains might had a slight preference in the face-on or co-existence of the face-on and other tiled chain orientations[4] driven by the driving force from the vertical surface separation of P3HT-b-P3TEGT or P3HT-b-P3TEGT:Li^+.

---------- Figure 2 ----------

The morphology of the active layer was critical to determine the performance of BHJ PSCs. With large interfacial area and bicontinuous vertical distribution of active layer components, the charge separation from donor copolymer to acceptor fullerene derivative could be enhanced and charge carriers collection from the active layer to respective electrode also be maximized. We used atomic force microscopy (AFM) in tapping mode to measure surface morphology of P3HT:$PC_{61}BM$ (1:1, w/w) with various H4T1 concentrations (height images in **Figure S4**) and H4T1:Li^+ (three-dimensional images in **Figure 3**). In addition, AFM images were also examined to elucidate the effect of H4T1 or H4T1:Li^+ on the phase separation of P3HT:$PC_{61}BM$ thin films. The surface morphology of pristine P3HT:$PC_{61}BM$ demonstrated a fine phase separation and bicontinuous network image with 2.3 nm root-mean-square (RMS) roughness. Considering the pristine H4T1 films showed a 2.84 nm RMS, it could infer that increasing H4T1 concentration would lead triethylene glycol side chains aggregating on the surface of the active layer and the films exhibited rougher surface. However, adding the H4T1 led the film surface become flat and uniform with the RMS of 0.62, 0.68 and 1.62 nm for H4T1 concentrations of 0.2, 0.6 and 1.0 mg/mL, respectively. On the other hand, we also utilized AFM measurements to investigate the effect of the H4T1:Li^+ on the orientation and distribution of P3HT:$PC_{61}BM$ active layer components and surface morphology[47] shown in **Figure 4**. The added Li^+ ions could chelate with the triethylene glycol side chains of P3HT-b-P3TEGT and

drive the polymer chains to self-assemble into nanowire morphology, according to our previous work in ref. [41]. It was found a well-ordered lamellar structure of H4T1:Li^+ covered P3HT:$PC_{61}BM$ active layer surface at the concentrations of 0.06 mg/mL and 0.18 mg/mL of Li^+ salt, resulting from the Li^+ ions driving the diblock copolymer chains into nanowires on the surface of the active layer[48]. Furthermore, uniform film morphology with 1.88 and 1.59 nm RMS induced by vertical surface segregation of triethylene glycol side chains of polythiophenes was observed during spin coating. However, further increasing of the concentration of H4T1:Li^+, large aggregations gradually appeared on the surface with RMS of 2.78 and 2.92 nm, and even the well-ordered lamellar structures disappeared.

---------- Figure 3 ----------

---------- Figure 4 ----------

We fabricated the inverted devices based on P3HT:$PC_{61}BM$:Li^+ and P3HT:$PC_{61}BM$:H4T1:Li^+ active layers to investigate the effect of Li^+ doping on device performance. The effects of different Li^+ concentrations in P3HT:$PC_{61}BM$ and P3HT:$PC_{61}BM$:H4T1 solutions on the device performance were studied and the device parameters were plotted in **Figure 5** as functions of Li^+ concentration. The *J-V* curves of these devices were showed in **Figure S5** and the correlated parameters were summarized in **Table S1**. All parameters of devices based on P3HT:$PC_{61}BM$:Li^+ dropped sharply with the concentration of Li^+ boosting. However, the parameters of devices based on P3HT:$PC_{61}BM$:H4T1:Li^+ first rose and then decreased gradually with the increase of Li^+ concentration. Compared with P3HT:$PC_{61}BM$:Li^+ device, the better performance and stability of the device based on P3HT:$PC_{61}BM$:H4T1:Li^+ was mainly due to the chelation of triethylene glycol side chains of H4T1 with Li^+ ions, which could drive the H4T1 diblock copolymer chains into nanowires and to migrate onto the surface of active layer. On the contrary, the addition of Li^+ into P3HT:$PC_{61}BM$ might not form an efficient anode buffer layer and resulted in dramatic decrease of PCE. The results indicated that the photovoltaic properties of BHJ PSCs could be easily improved by introducing P3HT-b-P3TEGT:Li^+ into active layer system[10]. On the other hand, the dark *J-V* characteristics of devices based on active layer P3HT:$PC_{61}BM$, P3HT:$PC_{61}BM$:Li^+, P3HT:$PC_{61}BM$:H4T1 or P3HT:$PC_{61}BM$:H4T1:Li^+ in range of -2 V to 2 V were obtained (**Figure S6)**. Obviously, adding a small amount of Li^+ ions into P3HT:$PC_{61}BM$ solution, the dark *J-V* curve presented a

relatively large leakage current density. However, the device with P3HT:PC_{61}BM:H4T1 containing Li^+ ions showed significantly suppressed leakages, resulting in best photovoltaic performance. More importantly, the low dark current densities of device based on P3HT:PC_{61}BM:H4T1:Li^+ indicated that the larger open-circuit voltage (V_{oc}) could be obtained in the inverted device with vertical phase separated buffer layer, compared with those without the nanoscale buffer layer. Towards the end, the *J-V* curves of devices were modeled with an equivalent circuit, and a single diode was consisted with shunt resistance (R_{SH}) and series resistance (R_S). The addition of a parallel photocurrent source, J_{ph}, resulted in the well-known equation:

$$J = J_0\left[\exp\left(\frac{q\left(V - R_S AJ\right)}{nkT}\right) - 1\right] + \frac{V - R_S AJ}{R_{SH} A} - J_{ph}\left(V\right)$$

where *k* represents Boltzmann's constant, *T* represents the temperature, *q* represents the electron charge, and J_{ph} represents the voltage-dependent photocurrent. When the condition is open circuit (J=0) and $J_{ph} = J_{sc}$, V_{oc} could be written as

$$V_{oc} \approx \frac{nkT}{q}\ln\left(\frac{J_{sc}}{J_0}\right)$$

The J_0 represents reverse dark current density. The higher V_{oc} could be obtained for the lower J_0 according to this equation. Therefore, it exhibited higher V_{oc} of the inverted devices with buffer layer than those devices without the buffer layer.

---------- Figure 5 ----------

To further analyze the reason for the improvement of device performance, we processed UV photoelectron spectroscopy (UPS) measurement to study the interfacial dipole effect provided by P3HT-b-P3TEGT and P3HT-b-P3TEGT:Li^+ self-assembled interfacial layer between active layer and Ag anode electrode. The UPS profiles of P3HT:PC_{61}BM:H4T1/Ag as function of H4T1 concentration and P3HT:PC_{61}BM:H4T1:Li^+(0.6 mg/mL H4T1 blending with 0.18 mg/mL Li^+ ions)/Ag were displayed in **Figure 6**. As measured from UPS, the WFs of Ag were shifted by 0.67, 0.81, 0.82 and 0.98 eV for 0.2, 0.6, 1.0 mg/mL H4T1 and H4T1:Li^+, respectively, indicating that increasing the amounts of P3HT-b-P3TEGT could enhance interfacial contact and raise WF of Ag electrode, especially upon adding P3HT-b-P3TEGT:Li^+. The "metal-on-organic" interfaces was more complicated[49-50], the rise in the effective WF of Ag

might attribute to the interfacial modification effect, originating from the vertical surface segregation of triethylene glycol side chains of P3HT-b-P3TEGT or P3HT-b-P3TEGT:Li^+ during spin coating process. The modification effect provided by P3HT-b-P3TEGT or P3HT-b-P3TEGT:Li^+ might result in the rise of WF of anode electrode and further allowed holes to be collected by the anode electrode more easily, hence, might lead to the improvement of J_{sc} and V_{oc} of device[10]. On the other hand, the WF of P3HT:PC_{61}BM:H8T1/Ag and P3HT:PC_{61}BM:H2T1/Ag were also shifted by 0.77 and 0.72 eV for the saturated point of ~ 1.2 mg/mL and ~ 0.3 mg/mL, compared with the film with 5 nm Ag deposited on the active layer without the addition of P3HT-b-P3TEGT. **Figure 6** represented the band energy diagram in relation to the relative energy levels of devices. More importantly, comparing with other devices, the experimental value observed for P3HT:PC_{61}BM:H4T1:Li^+/Ag thin film (5.18 eV) was very close to the HOMO energy level of P3HT or PBDTTT-C-T donor, which might be more favorable and responsible for the hole collection compared with the P3HT:PC_{61}BM:H8T1/Ag (4.97 eV), P3HT:PC_{61}BM:H4T1/Ag (5.01 eV) and P3HT:PC_{61}BM:H2T1/Ag (4.92 eV). On the other hand, the P3HT-b-P3TEGT could increase the energy level and passivate surface defects of MoO_3 by interfacial modification originating from triethylene glycol side chains of diblock copolymer in **Figure 6**, which might be beneficial for the energy level matching with Ag electrode and the improvement of J_{sc}[51].

---------- **Figure 6** ----------

The formation of interfacial modification and enhancement of WF of anode electrode induced by triethylene glycol side chains of P3HT-b-P3TEGT and P3HT-b-P3TEGT:Li^+ were expected to promote the exciton dissociation and increase the hole-carrier collection[52]. $J^{0.5}$-V characteristics of hole-only devices were fabricated to assess the hole mobility with a structure of ITO/PEDOT:PSS/active layer/MoO_3/Au, by using the space charge-limited-current (SCLC) model according to the Mott-Gurney equation (detail description of the mobility measurement was provided in **Supporting Information**)[53-55]. As plotted in **Figure S7**, hole mobility of the devices increased from 1.68×10^{-4} cm^2 V^{-1} s^{-1} to 2.78×10^{-4} cm^2 V^{-1} s^{-1}, 5.77×10^{-4} cm^2 V^{-1} s^{-1} and 1.15×10^{-3} cm^2 V^{-1} s^{-1} (**Table S3**) after insertion of PEDOT:PSS as HTL or introducing of P3HT-b-P3TEGT or P3HT-b-P3TEGT:Li^+ in P3HT:PC_{61}BM active layer at an applied voltage of 1 V, respectively, compared with the device without HTL. The results implied that the

incorporation of P3HT-b-P3TEGT or P3HT-b-P3TEGT:Li^+ into active layer would form a self-assembled HTL interlayer, resulting in the increase of the hole mobility and a more balanced charge transport in the devices. And on the other hand, the self-assembled interlayer could also reduce the thickness of device, reduce contact resistance and increase the electrical conductivity of inverted devices, which were beneficial for the improvement of device efficiency (The relevant results of R_s and R_{sh} shown in **Table 1** and **Table S2**).

The photovoltaic performance of devices based on ITO/ZnO/active layer/Ag (or MoO_3/Ag) inverted device structures by introducing P3HT-b-P3TEGT or P3HT-b-P3TEGT:Li^+ into the P3HT:$PC_{61}BM$ or PBDTTT-C-T:$PC_{71}BM$ active layers was studied. Devices were fabricated by spin-casting the active layer blends from DCB solution atop the ZnO interface layer on glass substrates patterned with indium tin oxide (ITO), followed by the deposition of 90 nm Ag or MoO_3 (6 nm)/Ag (90 nm) anode electrode. The overall ratio of polymer donors and fullerenes remained at 1:1 (wt%) with a fixed concentration of P3HT at 20 mg/mL. The detail information of the device fabrication and characterization was provided in **Supporting Information**. Current density-voltage (*J-V*) characteristics of the devices measured under AM 1.5G irradiation were shown in **Figure 7**. And the resulting J_{sc}, V_{oc}, FF and PCE values, determined from the *J-V* curves, were summarized in **Table 1** and **Table S2**. We could observe a better device performance when applying the MoO_3/Ag anode electrode mainly due to the high conductivity of MoO_3 and decrease of the energy level (**Figure 6**) and surface defects of MoO_3 by interfacial modification between triethylene glycol side chains of diblock copolymer and MoO_3. Firstly, the P3HT and $PC_{61}BM$ systems blended with P3HT-b-P3TEGT or P3HT-b-P3TEGT:Li^+ were selected as the active layer components. We optimized the device properties by changing the concentration of P3HT-b-P3TEGT and found that the optimized concentration is 1.2 mg/mL, 0.6 mg/mL and 0.3 mg/mL, for H8T1, H4T1 and H2T1 in sequence (**Table 1**, **Table S2** and **Figure 7**). When the amount of P3HT-b-P3TEGT was over the optimized concentration, the FF and J_{sc} largely decreased due to excessive segregation of P3HT-b-P3TEGT polymer chains at the top of the active layer, thus interrupting the holes transport. Then Li^+ was added into the P3HT:$PC_{61}BM$:P3HT-b-P3TEGT system at the optimized concentration of P3HT-b-P3TEGT. Surprisingly, relative to the device of ITO/ZnO/P3HT:$PC_{61}BM$/PEDOT:PSS/Ag, the incorporation of P3HT-b-P3TEGT or P3HT-b-P3TEGT:Li^+ in the active layer gave the increase

of J_{sc}, V_{oc} and FF, and consequently the PCE enhanced from 2.3 % to 3.4 % for ITO/ZnO/P3HT:PC_{61}BM:H4T1/Ag device, 3.6 % for ITO/ZnO/P3HT:PC_{61}BM:H4T1:Li^+/Ag. Encouragingly, the PCE of device could further be boosted to 3.4%, 3.9 % and 2.6% for H8T1, H4T1 and H2T1 addition in ITO/ZnO/P3HT:PC_{61}BM:P3HT-b-P3TEGT/MoO_3/Ag device structures, and even 3.9%, 4.2 % and 3.9% for H8T1:Li^+, H4T1:Li^+ and H2T1:Li^+ addition in ITO/ZnO/P3HT:PC_{61}BM:P3HT-b-P3TEGT:Li^+/MoO_3/Ag device structures.

The EQE values for the devices based on ITO/ZnO/P3HT:PC_{61}BM:P3HT-b-P3TEGT (or P3HT-b-P3TEGT:Li^+)/Ag (or MoO_3/Ag) were over 70 % in the range of 450 nm to 625 nm, which were much higher than the ITO/ZnO/P3HT:PC_{61}BM/PEDOT:PSS/Ag device (**Figure 8**). Besides, the lower response at short wavelength may originate from the vertical dispersion of the active layer components and the reflection mode from the cathode electrode, resulting in more light absorption of the donor material. The EQE results agreed well with the J_{sc} results. On the other hand, the enhancement in J_{sc} of BHJ PSCs could be attributed to the greater light reflection and the UV-filter effect imposed by P3HT-b-P3TEGT:Li^+ interfacial layer on active layer surface of the device, indicating there was a strong optical interference effect provided by P3HT-b-P3TEGT:Li^+ (**Figure 8**). Besides, the increase of V_{oc} was attributed to the better interfacial contact between active layer and Ag (or MoO_3/Ag) anode electrode because P3HT-b-P3TEGT or P3HT-b-P3TEGT:Li^+ could vertical phase separate into the top of active layer acting as the buffer layer. The ideal vertical component distribution morphology of the active layer originating from the driving force of P3HT-b-P3TEGT or P3HT-b-P3TEGT:Li^+, which spontaneously segregated on the surface of active layer during spin-coating process, could increase the charge transport and collection efficiency, consequently, enhance J_{sc} and V_{oc} of the devices. In addition, it should be noted we could observe hysteresis effect in *J-V* curves of devices with the addition of Li ions. While testing the J-V curves of devices with addition of Li ions, it presented normal at the first time but degenerative immediately in succeeding tests, but then became normal performance again after a period of time.

Overall, the improvement of the photovoltaic performance of the PSCs by introducing P3HT-b-P3TEGT or P3HT-b-P3TEGT:Li^+ into the active layer should benefit from better ohmic contact, higher electrical conductivity, the formation of interfacial modification and the vertical phase separation morphology induced by the spontaneous migration of P3HT-b-P3TEGT to the

active layer surface. The research paved a way for the further development of PSC BHJ solar cells with high efficiency by introducing diblock copolymer with triethylene glycol side chains into the active layer system. So, we further investigate the effect of P3HT-b-P3TEGT or P3HT-b-P3TEGT:Li^+ on other active layer system. The second type of device was based on a low-bandgap 2D-conjugated polymer poly(4,8-bis(5-(2-ethyl-hexyl)-thiophene-2-yl)-benzo[1,2-b:4,5-b']dithiophene-alt-alkylcarbonyl-thieno[3,4-b]thiophene) (PBDTTT-C-T) [56-58] and the [6,6]-phenyl-C_{71}-butyric acid methyl ester ($PC_{71}BM$), i.e. PBDTTT-C-T/$PC_{71}BM$ active layer system, applying the same inverted device structure. Interestingly, the devices also showed the enhanced photovoltaic performance and the PCE could reach 6.9%, 7.3% and 7.1% for adding H8T1, H4T1 and H2T1, and 6.4%, 6.7% and 6.6% for adding H8T1:Li^+, H4T1:Li^+ and H2T1:Li^+ respectively, from 4.7% of pristine device without any buffer layers (**Table 1**, **Table S2** and **Figure 7**). It should be mentioned that there existed a drop of PCE for the PBDTTT-C-T/$PC_{71}BM$ system upon adding P3HT-b-P3TEGT:Li^+ compared with the same system blended with P3HT-b-P3TEGT. The detailed mechanism was not very clear at present stage. The EQE data were presented in **Figure 8**. Observing from AFM images of PBDTTT-C-T:$PC_{71}BM$, PBDTTT-C-T:$PC_{71}BM$:P3HT-b-P3TEGT and PBDTTT-C-T:$PC_{71}BM$:P3HT-b-P3TEGT:Li^+, well phase separation of donor/acceptor appeared on the active layer surface after introducing P3HT-b-P3TEGT into active layer, while a larger and more orderly nanofiber appeared after introducing P3HT-b-P3TEGT:Li^+ (**Figure S8**). Furthermore, the incorporation of the P3HT-b-P3TEGT or P3HT-b-P3TEGT:Li^+ into active layer and formation of self-assembled buffer layer between active layers and anode electrodes during the spin-coating process could promote the stability of the inverted devices (**Figure 8**). All the devices (no encapsulation) were located in air continuously at room temperature and PCEs remained above 85% of the original value for P3HT-b-P3TEGT, 75% for P3HT-b-P3TEGT:Li^+ and 10% for PEDOT:PSS even after exposing to air for more than 4 weeks, no matter whether the devices with or without MoO_3 layer.

---------- Figure 7 ----------

---------- Figure 8 ----------

Conclusions

The device performance and stability could be enhanced by the application of polythiophene conjugated diblock copolymer containing polythiophene derivative segments whose side chain was triethylene glycol (P3HT-b-P3TEGT) or P3HT-b-P3TEGT chelated with Li^+ (P3HT-b-P3TEGT:Li^+), in the active layer system. Due to the spontaneously vertical migration of P3HT-b-P3TEGT or P3HT-b-P3TEGT:Li^+ to the surface of active layer during the spin-coating process and formation of self-assembled anode buffer layer, a vertical distribution of components in active layer and orderly arrangement of donor polymer chains were obtained at the same time, which was the ideal BHJ morphology allowing holes and electrons moving to the anode and cathode electrode more efficiently, respectively. In addition, the self-assembled anode buffer layer could provide the interfacial modification between active layer and Ag (or MoO_3/Ag) anode electrodes, enhance the WF of anode electrode, increase the electrical conduction of the device, and consequently remarkably improve the device performance and stability. The PCE increased to 7.3 % for devices based on PBDTTT-C-T:$PC_{71}BM$. Such research paved a way for the further development of highly efficient and stable PSC BHJ solar cells by simple introducing conjugated diblock copolymer with triethylene glycol side chain into the active layer system.

Acknowledgements

The financial supports for this work are provided by the National Natural Science Foundation of China (51273088 and 51302130) and Doctoral Programs Foundation of Ministry of Education of China (Grants 20133601110004 and 20133601120006). Yueqin Shi and Licheng Tan contributed equally to this work.

Supporting Information Available

Text giving the detailed experimental procedures. This information is available free of charge via the Internet at http://pubs.rsc.org/.

References:

1. S. Albrecht, S. Janietz, W. Schindler, J. Frisch, J. Kurpiers, J. Kniepert, S. Inal, P. Pingel, K. Fostiropoulos, N. Koch and D. Neher, *J. Am. Chem. Soc.,* 2012, **134,** 14932.

2. J. Yuan, Z. Zhai, H. Dong, J. Li, Z. Jiang, Y. Li and W. Ma, *Adv. Funct. Mater.,* 2013, **23,** 885.

3. J. Peet, J. Y. Kim, N. E. Coates, W. L. Ma, D. Moses, A. J. Heeger and G. C. Bazan, *Nat.*

Mater., 2007, **6,** 497.

4. Y. Kim, H. R. Yeom, J. Y. Kim and C. Yang, *Energy Environ. Sci.,* 2013, **6,** 1909.

5. K. R. Graham, P. M. Wieruszewski, R. Stalder, M. J. Hartel, J. Mei, F. So and J. R. Reynolds, *Adv. Funct. Mater.,* 2012, **22,** 4801.

6. Z. He, C. Zhong, S. Su, M. Xu, H. Wu and Y. Cao, *Nat. Photonics,* 2012, **6,** 591.

7. L. Dou, J. You, J. Yang, C.-C. Chen, Y. He, S. Murase, T. Moriarty, K. Emery, G. Li and Y. Yang, *Nat. Photonics,* 2012, **6,** 180.

8. Y. Sun, J. H. Seo, C. J. Takacs, J. Seifter and A. J. Heeger, *Adv. Mater.,* 2011, **23,** 1679.

9. A. K. K. Kyaw, D. H. Wang, D. Wynands, J. Zhang, T.-Q. Nguyen, G. C. Bazan and A. J. Heeger, *Nano Lett.,* 2013, **13,** 3796.

10. K. Yao, L. Chen, X. Chen and Y. Chen, *Chem. Mater.,* 2013, **25,** 897.

11. J. You, L. Dou, K. Yoshimura, T. Kato, K. Ohya, T. Moriarty, K. Emery, C.-C. Chen, J. Cao, G. Li and Y. Yang, *Nat. Commun.,* 2013, **4,** 1446.

12. W. W. Li, A. Furlan, K. H. Hendriks, M. M. Wienk and R. A. J. Janssen, *J. Am. Chem. Soc.,* 2013, **135,** 5529.

13. J. Zhou, Y. Zuo, X. Wan, G. Long, Q. Zhang, W. Ni, Y. Liu, Z. Li, G. He, C. Li, B. Kan, M. Li and Y. Chen, *J. Am. Chem. Soc.,* 2013, **135,** 8484.

14. A. K. K. Kyaw, D. H. Wang, V. Gupta, J. Zhang, S. Chand, G. C. Bazan and A. J. Heeger, *Adv. Mater.,* 2013, **25,** 2397.

15. C. Cabanetos, A. E. Labban, J. A. Bartelt, J. D. Douglas, W. R. Mateker, J. M. J. Fréchet, M. D. McGehee and P. M. Beaujuge, *J. Am. Chem. Soc.,* 2013, **135,** 4656.

16. H. J. Son, L. Y. Lu, W. Chen, T. Xu, T. Y. Zheng, B. Carsten, J. Strzalka, S. B. Darling, L. X. Chen and L. P. Yu, *Adv. Mater.,* 2013, **25,** 838.

17. J. A. Bartelt, Z. M. Beiley, E. T. Hoke, W. R. Mateker, J. D. Douglas, B. A. Collins, J. R. Tumbleston, K. R. Graham, A. Amassian, H. Ade, J. M. J. Fréchet, M. F. Toney and M. D. McGehee, *Adv. Energy Mater.,* 2013, **3,** 364.

18. S. Qu, M. Li, L. Xie, X. Huang, J. Yang, N. Wang and S. Yang, *ACS Nano,* 2013, **7,** 4070.

19. X. Wan, G. Long, L. Huang and Y. Chen, *Adv. Mater.,* 2011, **23,** 5342.

20. S.-S. Li, K.-H. Tu, C.-C. Lin, C.-W. Chen and M. Chhowalla, *ACS Nano,* 2010, **4,** 3169.

21. J. Liu, Y. Xue, Y. Gao, D. Yu, M. Durstock and L. Dai, *Adv. Mater.,* 2012, **24,** 2228.

22. S.-Y. Ku, M. A. Brady, N. D. Treat, J. E. Cochran, M. J. Robb, E. J. Kramer, M. L. Chabinyc and C. J. Hawker, *J. Am. Chem. Soc.,* 2012, **134,** 16040.

23. G. Li, Y. Yao, H. Yang, V. Shrotriya, G. Yang and Y. Yang, *Adv. Funct. Mater.,* 2007, **17,** 1636.

24. Q. Wei, M. Mukaida, Y. Naitoh and T. Ishida, *Adv. Mater.,* 2013, **25,** 2831.

25. K. R. Graham, P. M. Wieruszewski, R. Stalder, M. J. Hartel, J. Mei, F. So and J. R. Reynolds, *Adv. Funct. Mater.,* 2012, **22,** 4801.

26. F. Etzold, I. A. Howard, N. Forler, D. M. Cho, M. Meister, H. Mangold, J. Shu, M. R. Hansen, K. Müllen and F. Laquai, *J. Am, Chem. Soc.,* 2012, **134,** 10569.

27. C. Renaud, S.-J. Mougnier, E. Pavlopoulou, C. Brochon, G. Fleury, D. Deribew, G. Portale, E. Cloutet, S. Chambon, L. Vignau, and G. Hadziioannou, *Adv. Mater.,* 2012, **24***,* 2196.

28. F.-C. Chen, H.-C. Tseng and C.-J. Ko, *Appl. Phys. Lett.,* 2008, **92,** 103316.

29. X. Guo, C. Cui, M. Zhang, L. Huo, Y. Huang, J. Hou and Y. Li, *Energy Environ. Sci.,* 2012, **5,** 7943.

30. J. Peet, M. L. Senatore, A. J. Heeger and G. C. Bazan, *Adv. Mater.,* 2009, **21,** 1521.

31. Z. Xu, L.-M. Chen, G. Yang, C.-H. Huang, J. Hou, Y. Wu, G. Li, C.-S. Hsu and Y. Yang, *Adv. Funct. Mater.,* 2009, **19,** 1227.

32. K. H. Lee, P. E. Schwenn, A. R. G. Smith, H. Cavaye, P. E. Shaw, M. James, K. B. Krueger, I. R. Gentle, P. Meredith and P. L. Burn, *Adv. Mater.,* 2011, **23,** 766.

33. S.-C. Chien, F.-C. Chen, M.-K. Chung and C.-S. Hsu, *J. Phys. Chem. C,* 2012, **116,** 1354.

34. J. H. Seo, A. Gutacker, Y. Sun, H. Wu, F. Huang, Y. Cao, U. Scherf, A. J. Heeger and G. C. Bazan, *J. Am. Chem. Soc.,* 2011, **133,** 8416.

35. R. Po, C. Carbonera, A. Bernardi and N. Camaioni, *Energy Environ. Sci.,* 2011, **4,** 285.

36. J. W. Jung, J. W. Jo and W. H. Jo, *Adv. Mater.,* 2011, **23,** 1782.

37. F.-C. Chen, M.-K. Chuang, S.-C. Chien, J.-H. Fang and C.-W. Chu, *J. Mater. Chem.,* 2011, **21,** 11378.

38. Q. Tai, J. Li, Z. Liu, Z. Sun, X. Zhao and F. Yan, *J. Mater. Chem.,* 2011, **21,** 6848.

39. F.-C. Chen and S.-C. Chien, *J. Mater. Chem.,* 2009, **19,** 6865.

40. M. Jeffries-EL, G. Sauvé and R. D. McCullough, *Adv. Mater.,* 2004, **16,** 1017.

41. Y. Shi, L. Tan, L. Chen and Y. Chen, *Macromolecules,* 2014, **47,** 1757.

42. G. H. Jun, S. H. Jin, B. Lee, B. H. Kim, W.-S. Chae, S. H. Hong and S. Jeon, *Energy Environ. Sci.,* 2013, **6,** 3000.

43. R. Xiong, G. Sang, X. Yan, G. Zhang, Q. Xu and H. Zhang, *Chem. Commun.,* 2013, **49,** 2046.

44. S. Ren, L.-Y. Chang, S.-K. Lim, J. Zhao, M. Smith, N. Zhao, V. Bulović, M. Bawendi and S. Gradečak, *Nano Lett.,* 2011, **11,** 3998.

45. S.-H. Liao, Y.-L. Li, T.-H. Jen, Y.-S. Cheng and S.-A. Chen, *J. Am. Chem. Soc.,* 2012, **134,** 14271.

46. Y. Geng, Q. Wei, K. Hashimoto and K. Tajima, *Chem. Mater.,* 2011, **23,** 4257.

47. N. Gao, Y. Yan, X. Chen and D. J. Mee, *Langmuir,* 2012, **28,** 12256.

48. E. Lee, B. Hammer, J.-K. Kim, Z. Page, T. Emrick and R. C. Hayward, *J. Am. Chem. Soc.,* 2011, **133,** 10390.

49. H. Ishii, K. Sugiyama, E. Ito and K. Seki, *Adv. Mater.,* 1999, **11,** 972.

50. J. Hwang, A. Wan and A. Kahn, *Mater. Sci. Eng. R-Rep,* 2009, **64,** 1.

51. N. S. Arul, D. Y. Yun, D. U. Lee and T. W. Kim, *Nanoscale,* 2013, **5,** 11940.

52. Y. Yuan, T. J. Reece, P. Sharma, S. Poddar, S. Ducharme, A. Gruverman, Y. Yang and J. Huang, *Nat. Mater.,* 2011, **10***,* 296.

53. Y. Liu, X. Wan, F. Wang, J. Zhou, G. Long, J. Tian and Y. Chen, *Adv. Mater.,* 2011, **23,** 5387.

54. G. Zhao, Y. He, Z. Xu, J. Hou, M. Zhang, J. Min, H.-Y. Chen, M. Ye, Z. Hong, Y. Yang and Y. Li, *Adv. Funct. Mater.,* 2010, **20,** 1480.

55. Y.-J. Cheng, C.-H. Hsieh, P.-J. Li and C.-S. Hsu, *Adv. Funct. Mater.,* 2011, **21,** 1723.

56. L. Huo, S. Zhang, X. Guo, F. Xu, Y. Li and J. Hou, *Angew. Chem. Int. Ed.,* 2011, **50,** 9697.

57. L. Ye, S. Zhang, L. Huo, M. Zhang and J. Hou, *Acc. Chem. Res.,* 2014, **47,** 1595.

58. L. Ye, S. Zhang, W. Zhao, H. Yao, J. Hou, *Chem. Mater.,* 2014, **26,** 3603.

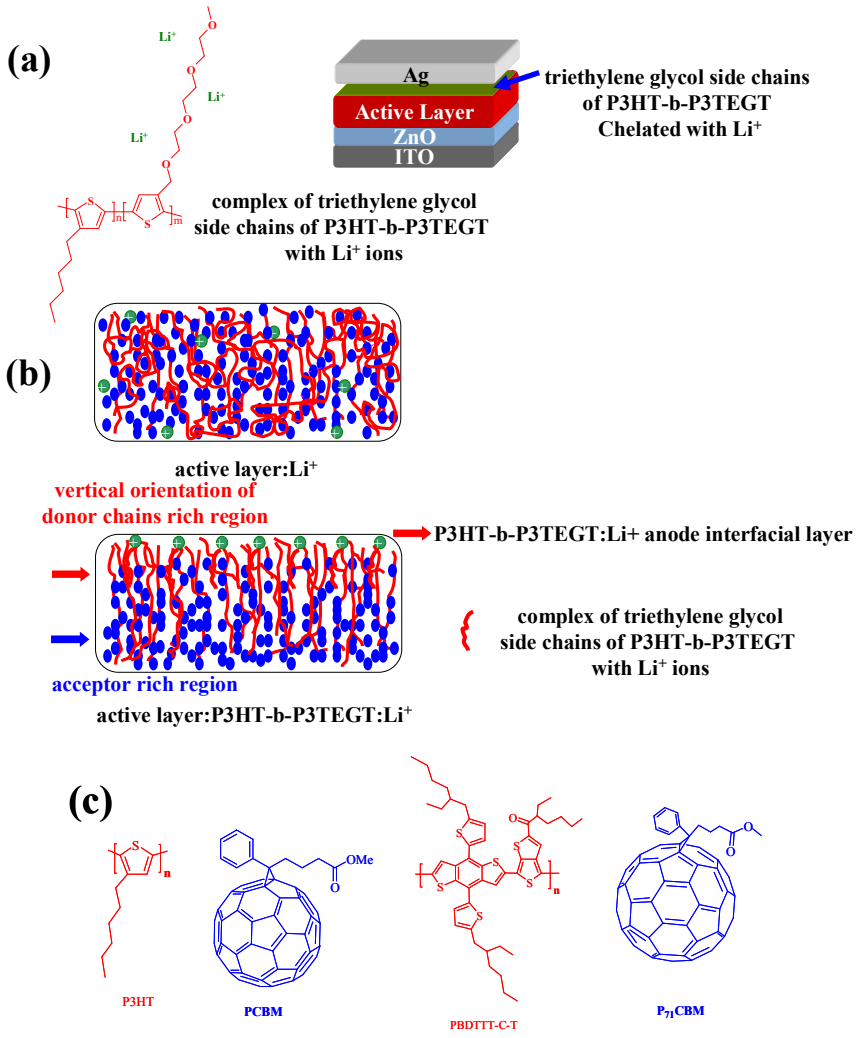

Scheme 1. Schematic illustration of (a) inverted bulk heterojuction polymer solar cells device based on vertical segregation of P3HT-b-P3TEGT chelated with Li^+ on the active layer surface, (b) the morphology of active layer:Li^+ and active layer:P3HT-b-P3TEGT:Li^+, (c) the chemical structures of donor and acceptor materials in active layer used in this study.

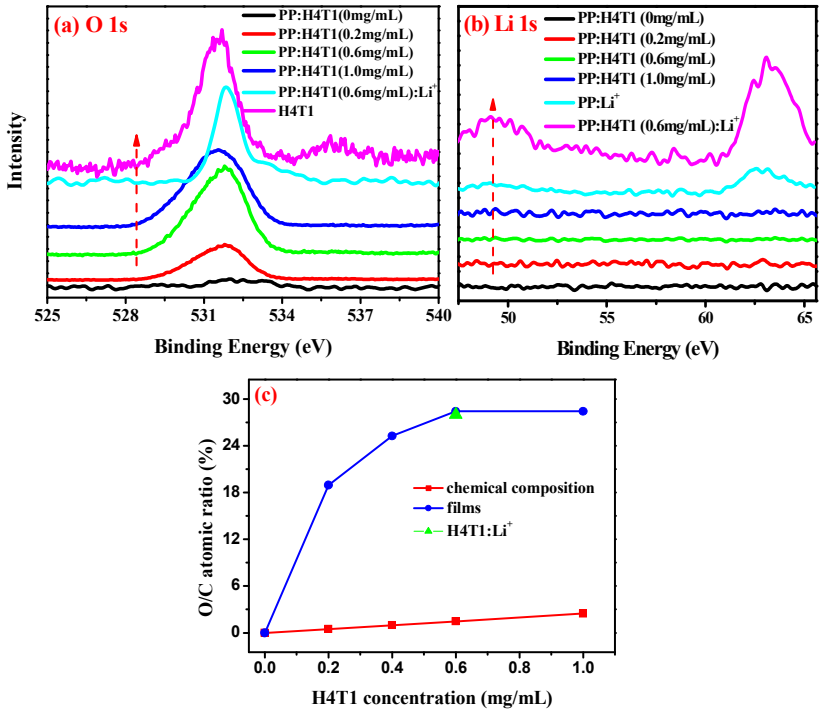

Figure 1. (a) O 1s region and (b) Li 1s of X-ray photoelectron spectroscopy (XPS) profiles of the surface of P3HT:$PC_{61}BM$ (PP) films with different H4T1 concentrations, pure Li^+ ion, H4T1 and H4T1(0.6 mg/mL):Li^+. (c) O/C atomic ratio of the P3HT:$PC_{61}BM$:H4T1 (PP:H4T1) films and the PP:H4T1(0.6 mg/mL):Li^+ film surfaces measured by XPS and the O/C atomic ratio of PP:H4T1 solutions calculated from the polymer chemical compositions, as the function of H4T1 concentration.

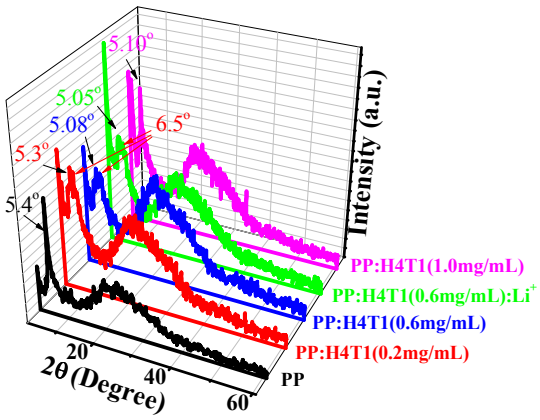

Figure 2. XRD patterns of P3HT:$PC_{61}BM$ (PP) blended with different concentration of H4T1 and 0.6 mg/mL H4T1 chelated with Li^+ films.

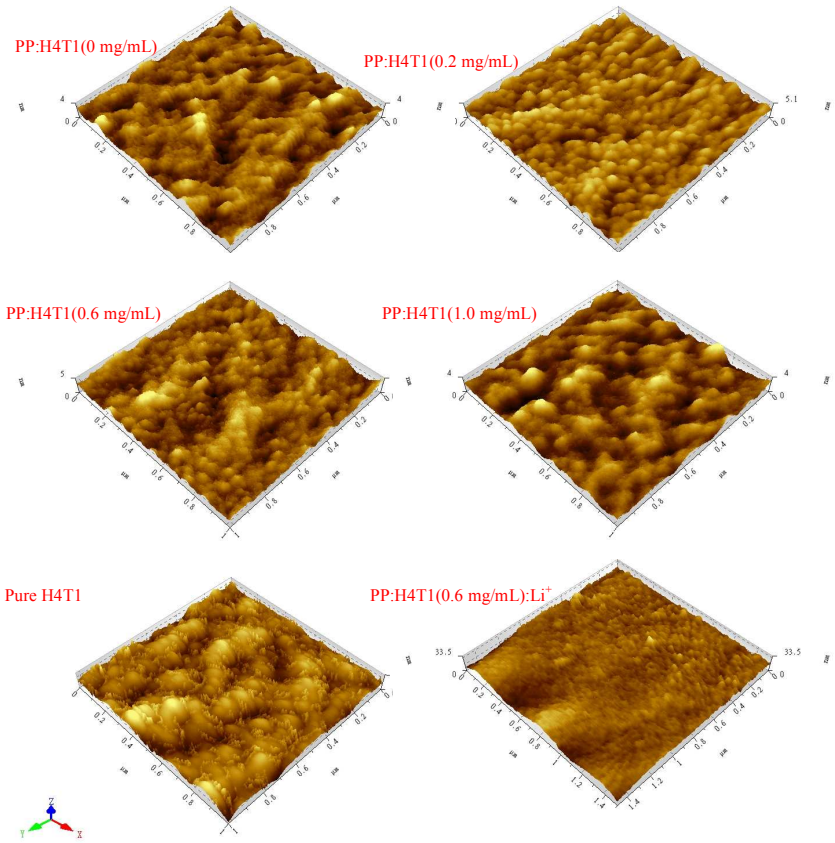

Figure 3. Three-dimensional atomic force microscopy (AFM) images of P3HT:$PC_{61}BM$ (PP) with various H4T1 concentration ranged from 0 mg/mL to 1.0 mg/mL, 0.6 mg/mL H4T1 chelated with Li^+ and pristine H4T1 films. The image sizes were all 5 μm × 5 μm.

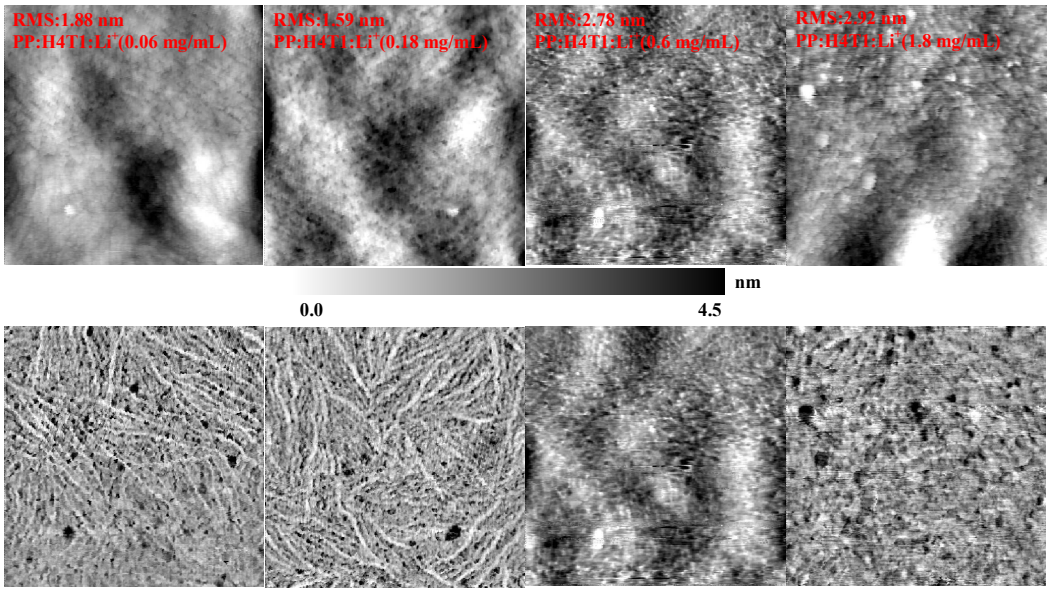

Figure 4. The height (above) and phase (below) atomic force microscopy (AFM) images of P3HT:$PC_{61}BM$ (PP) blended with H4T1:Li^+ with various Li^+ concentration range from 0.06 mg/mL to 1.8 mg/mL at the fixed H4T1 concentration of 0.6 mg/mL. The image sizes were all 5 μm × 5 μm.

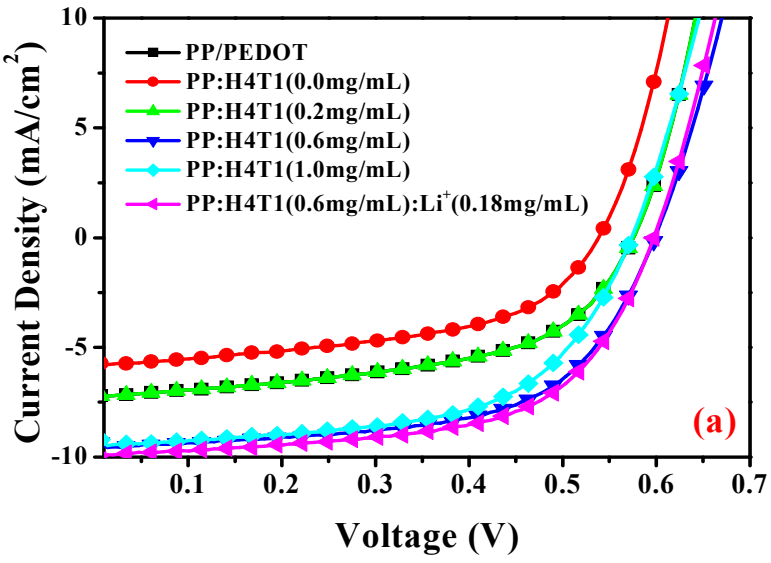

Figure 5. The photovoltaic parameters of the PSCs based on P3HT:$PC_{61}BM$ (PP) and P3HT:$PC_{61}BM$:H4T1 (PP:H4T1, 0.6 mg/mL H4T1) with various Li^+ concentration under illumination of AM 1.5G (100 mW/cm^2).

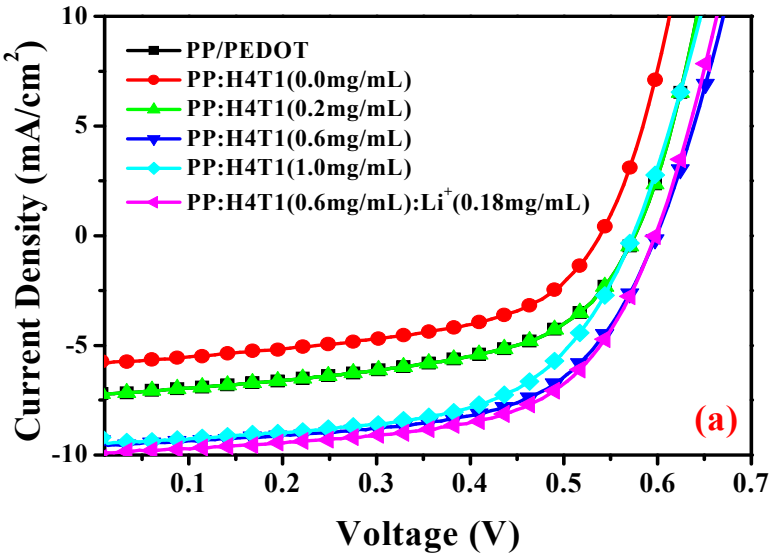

Figure 6. (a) The ultraviolet photoelectron spectroscopy (UPS) of 5 nm thick layer Ag films deposited on active layer (P3HT:$PC_{61}BM$) (PP) with various concentrations of P3HT-b-P3TEGT (H4T1) on the ITO substrate: 0.0mg/mL, 0.2 mg/mL, 0.6 mg/mL, 1.0 mg/mL and 0.6 mg/mL chelated with Li^+ salt; (b) The ultraviolet photoelectron spectroscopy (UPS) of 5 nm thick layer Ag films deposited on various diblock copolymers films surface; (c) The ultraviolet photoelectron spectroscopy (UPS) of pure MoO_3 and MoO_3 deposited on H4T1 diblock copolymers surface. (d) Schematic representation of band energy diagram for inverted BHJ PSCs devices based on different hole buffer layers vertical segregating on the active layer surface.

Table 1. Device performance parameters of inverted solar cells with different active layers by incorporating H4T1 at various concentrations or incorporating H4T1:Li^+.

Device[a,b]	J_{sc} (mA/cm^2)	V_{oc} (V)	FF (%)	PCE (%)	R_s ($\Omega\cdot$cm^2)	R_{sh} ($\Omega\cdot$cm^2)
ITO/ZnO/PP[c]/PEDOT:PSS/Ag	7.5	0.57	54	2.3±0.3	10.3	630
ITO/ZnO/PP[c]/Ag	6.07	0.53	50	1.6±0.2	12.9	268
ITO/ZnO/PP[c]:H4T1(0.2)[d]/Ag	7.5	0.57	53	2.3±0.2	9.3	396
ITO/ZnO/PP[c]:H4T1(0.6)[d]/Ag	9.74	0.59	59	3.4±0.2	5.1	310
ITO/ZnO/PP[c]:H4T1(1.0)[d]/Ag	9.52	0.57	58	3.1±0.2	6.7	598
ITO/ZnO/PP[c]:H4T1(0.6)[d]:Li^+(0.18)[e]/Ag	9.91	0.59	62	3.6±0.2	1.3	367
ITO/ZnO/PP[c]:H4T1(0.2)[d]/MoO_3/Ag	9.52	0.58	58	3.2±0.2	1.2	728
ITO/ZnO/PP[c]:H4T1(0.6)[d]/MoO_3/Ag	10.9	0.60	59	3.9±0.2	13.2	467
ITO/ZnO/PP[c]:H4T1(1.0)[d]/MoO_3/Ag	10.8	0.61	54	3.6±0.2	3.5	455
ITO/ZnO/PP[c]:H4T1(0.6)[d]:Li^+(0.18)[e]/MoO_3/Ag	11.2	0.60	62	4.2±0.2	1.4	372
ITO/ZnO/PBP[c]/Ag	11.39	0.73	57	4.7±0.3	4.5	170
ITO/ZnO/PBP[c]:H4T1(0.6)[d]/MoO_3/Ag	17.01	0.77	56	7.3±0.1	1.3	545
ITO/ZnO/PBP[c]:H4T1(0.6)[d]:Li^+(0.18)[e]/MoO_3/Ag	16.88	0.75	53	6.7±0.1	2.8	170

[a]All values represented averages from fifteen 0.04 cm^2 devices on a single chip. [b]Device structure: ITO/ZnO(20 nm)/active layer (150 nm)/MoO_3/Ag. [c]PP represented P3HT:$PC_{61}BM$ (PP) (1:1 w/w) with thermal annealing at 150 °C for 10 min and PBP represented PBDTTT-C-T:$PC_{71}BM$ (PBP) (1:1.5 w/w) with 3% DIO additive. [d]The values in the parentheses presented the concentrations (mg/mL) of H4T1 with different block ratios in the active layer solutions. [e]The values in the parentheses presented the concentrations (mg/mL) of Li^+ in the active layer solutions. All the MoO_3 layers were 6 nm.

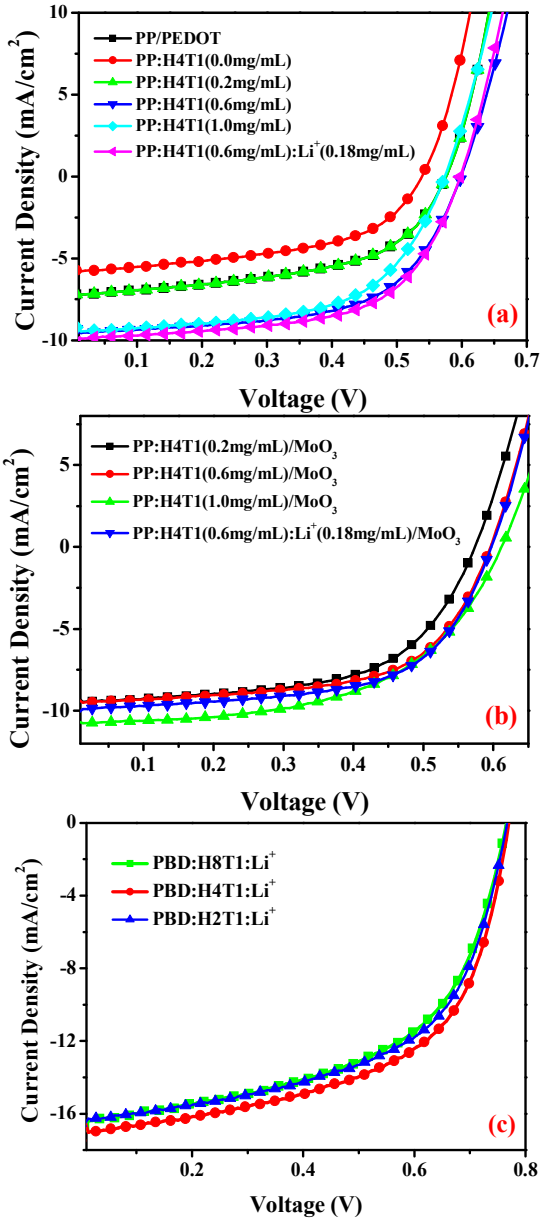

Figure 7. *J-V* curves of the PSCs based on P3HT:$PC_{61}BM$ (PP) with PEDOT:PSS as anode buffer layer or different H4T1 concentrations (from 0 to 1.0 mg/mL) and H4T1 (0.6 mg/mL):Li^+ (0.18 mg/mL) self-assembled buffer layer following (a) without and (b) with 6 nm MoO_3 layer under illumination of AM 1.5G, 100 mW/cm^2. (c) PSCs based on PBDTTT-C-T:$PC_{71}BM$ (PBP) (1:1.5 w/w, 3% DIO additive) with H8T1:Li^+, H4T1:Li^+ and H2T1:Li^+ anode buffer layers with MoO_3 layer under illumination of AM 1.5G, 100 mW/cm^2.

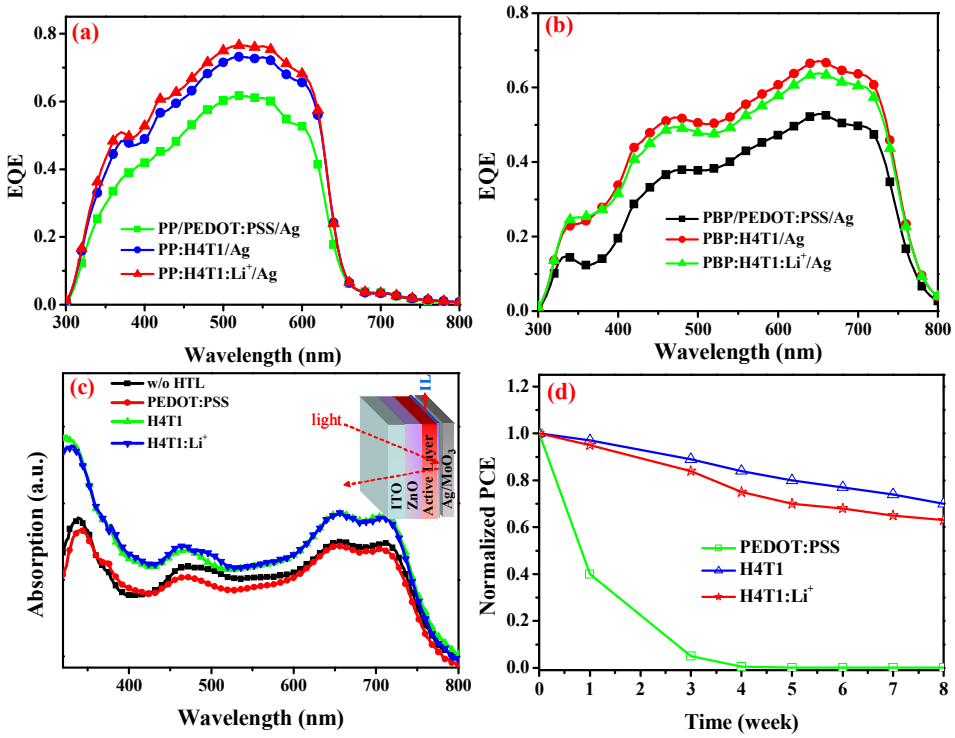

Figure 8. External quantum efficiency spectra of the PSCs based on (a) P3HT:$PC_{61}BM$ (PP) and (b) PBDTTT-C-T:$PC_{71}BM$ (PBP) with different self-assembly anode buffer layers, (c) the total absorption spectra in similar devices with different interfacial layer following with a 6 nm MoO_3 layer on the interfacial layer surface measured in the reflection geometry, the inset showing the device structure and (d) the normalized PCEs for inverted BHJ PSCs with PEDOT:PSS, P3HT-b-P3TEGT and P3HT-b-P3TEGT:Li^+ anode interfacial layer following with MoO_3 layer as a function of storage time in air under ambient conditions.

Highlights

Self-assembled Buffer Layer from Conjugated Diblock Copolymers with Ethyleneoxide Side Chains for High Efficiency Polymer Solar Cells

Yueqin Shi, Licheng Tan, Lie Chen, Yiwang Chen

A remarkable improvement in PCE of 7.3 % is obtained through spontaneously migrate of diblock copolymers during the spin process.

Graphical abstract